Debonding Mechanism of FRP Strengthened Flat Surfaces: Analytical Approach and Closed Form Solution.

Gabriele Milani [a], Ernesto Grande [b], Elisa Bertolesi*[c], Tommaso Rotunno [d], Mario Fagone [e].

[a] Department of Architecture, Built Environment and Construction Engineering (ABC), Politecnico di Milano, Piazza Leonardo da Vinci 32, 20133 Milan, Italy

[b] Department of Sustainability Engineering, University Guglielmo Marconi, Via Plinio 44, 00193 Rome, Italy

[c] Department of Civil and Environmental Engineering, Brunel University London, UB8 3PH Uxbridge, UK

[d] Dipartimento di Architettura (DiDA), Università degli Studi di Firenze, Piazza Brunelleschi 6, 50121 Florence, Italy

[e] Dipartimento di Ingegneria Civile e Ambientale (DICEA), Università degli Studi di Firenze, Piazza Brunelleschi 6, 50121 Florence, Italy

Keywords: Debonding Mechanisms, FRP composite materials, Closed form solution, Bond-slip model, Strengthening.

Abstract

Fiber Reinforced Polymer (FRP) composites represent an effective retrofitting strategy for the rehabilitation of masonry and concrete structures. The importance of adhesion between support and strengthening material is crucial and great research effort has been aimed at understanding this phenomenon from an analytical perspective. According to interfacial stress analysis, the debonding mechanism may be idealized and studied as an FRP–interface-support system with elastic FRP bonded to a brittle inelastic interface. In the present work, a fully analytical approach is developed to analyse the debonding mechanism of FRP strips applied to flat masonries providing a closed form solution characterized by few parameters governing the mathematical problem. Compared with other analytical methods, the present approach is advantageous in its closed form formulation, which allows the problem to be solved with a limited computational effort in a standard Matlab environment. The approach is benchmarked with two different sets of experimental results taken from the technical literature and from an ongoing investigation carried out by the authors. The results demonstrate the reliability of the method in analysing the debonding of FRP applied on flat masonry prisms.

1. Introduction

Nowadays it can be stated that Fibre Reinforced Polymer (FRP) composites have replaced traditionally repairing techniques for the strengthening of old or structurally deficient masonries [1]-[3]. FRPs present some common advantages with newly developed strengthening materials, such as FRCM / TRM composites, including ease of installation, design flexibility and high corrosion resistance [1]. In contrast to FRCM / TRM composites, FRPs offer a low weight-to-strength ratio, high stiffness, high tensile strength, thus leading to high ductility and strength enhancements. Although FRCM / TRM materials have some clear advantages in terms of compatibility with ancient supports, their failure mechanisms present some tricky aspects, such as multiple failure modes that involve fabric slippage, detachment from the supports and bundle tensile ruptures. Given the rather low tensile strength of the cementitious matrix, the long-term performance of these materials, especially when the matrix is cracked, is still being evaluated, as well as a complete procedure for deriving significant parameters for their design. Thus, the application of FRPs gained increasing popularity mainly thanks to their high versatility [4]-[7]. At the same time, their wide adoption shed light on one of their major features: the importance of adhesion between support and strengthening material, to which the performance of the entire system is entrusted [8]-[15]. When it comes to existing masonry structures, the quality of the bonding is of fundamental importance as different mechanical and geometric parameters of the structure to be reinforced can deeply affect the bond quality of the final installation. For such reason, researchers all over the world, focused on discovering the underlying causes of the loss of adhesion, predicting the final performance of FRP strengthening solutions and improving their adhesion characteristics [16]-[25]. A step towards a better understanding of the debonding phenomenon is represented by the huge number of experimental studies dealing with the debonding of FRPs from brittle supports (i.e. masonry and concrete) [1], [8]-[15]. Traditionally, bonding properties and debonding failures of FRP materials are investigated, even if with variable consistency, through three laboratory set-ups [1], [8]-[15]: (i) single lap, (ii) double lap and (iii) two-block double lap shear tests. Some peculiar conclusions can be drawn from all these investigations: (i) the influence of the type of support is confirmed, being the quality of the bond influenced by both its mechanical and physical properties. Considering the variety of masonry structures, usually built with locally available materials, this point is of crucial interest for the design of FRP reinforcement solutions. (ii) FRP debonding phenomena could be assimilated to a fracture mechanics Mode-II interface bonding loss event. Thus, the damage process is enclosed in a thin or thick layer at the interface between the reinforcing material and the support with decreasing participation of this latter as it moves away from the retrofitting area. The interfacial stress transfer phenomenon can be described fictitiously using a cohesive law or tau-slip relationship. The stress-slip law of the interface bond is usually described by a bi or tri linear model characterized by a linear elastic part upon reaching the peak tangential strength and followed by a descending softening branch until reaching a frictionless state or a residual friction strength [16]-[19],[24]-[26]. Piecewise linear bond-slip laws were found out mainly using strain sensor readings and inverse analysis, which allowed the calibration of their characteristic parameters too (i.e. peak tensile strength, tangential stiffness and post peak behavior). Therefore, the experimental tests confirmed the possibility of reducing the development of nonlinear detachment phenomena to an interface layer and the advantages inherent in this hypothesis encouraged researchers to follow this convenient modeling approach. Such approach was established as the dominant strategy not only for research purposes but also for the design of FRP composite strengthening solutions in current Italian and international guidelines [26]-[32]. Although a lack of consensus on the precise parametric dependence exists among different international guidelines [27]-[32], it is generally accepted that the mechanical properties of the support are a direct determinant of the bond-slip properties. Two different but equally worthy approaches are developed in the technical literature: (i) 2D/3D numerical models that consider perfectly bonded FRPs [21],[33],[34] or with elastic interfaces [35]-[37] and, (ii) analytical models [19],[23]-[26]. The first category [21],[33],[34] is often considered as a rough simplification of the adhesion properties of FRPs, which in those researches completely depend on the mechanical properties of the constituent materials. Usually, this approach is coupled with sophisticated material models (i.e. Concrete Damage Plasticity models) and a micro-mechanical modeling strategy that, in the authors' opinion, makes such approaches worth mentioning especially considering their practice-oriented feature. The focus of such works [21],[33]-[37] is indeed to provide an in-depth view of the failure modes of masonry assemblies and to explain, regardless of the adhesion quality, the implications of secondary parameters on the final performance of the installation, namely: geometry of the specimens, tensile and compressive properties of the constituent materials and their post-peak characteristics and damage propagation in the different components (e.g. mortar joints, bricks). Regardless of the complexity of the model which varies according to the strategy and hypothesis adopted, the aforementioned approaches offer several advantages such as the possibility to calibrate new bond–slip relationships, to compare the currently available ones using pseudo-experimental data generated by the FE models or to simplify the study of multiple related parameters [21],[33]-[36]. Another example of the possibilities that such approaches offer is represented by a simplified 1D FE model implemented into a Matlab environment proposed in [16] and later validated in [17],[18] against different experimental results, some of them on curved masonry pillars. The model simulates an FRP strip applied to a masonry substrate by means of a set of non-linear axial and shear springs, in which the latter are characterized by a bi-linear bond-slip interface law and the relationship between shear and normal springs typically obeys a Mohr-Coulomb behaviour. Apart from the extremely low computational burden, the model is easily generalizable -as already anticipated- to complex geometries such as curved supports [18]. Closed form analytical approaches represent a second branch of research in this context, driven by their extremely low computational cost and ease of adoption and utilization by everyone. Worth of special mention is the work presented in [38], in which a closed form analytical solution is presented to predict the debonding behaviour of FRP-to-concrete strengthening. Further to provide a strong theoretical background, the authors in [38], enrich the discussion by furnishing an experimental-based method to identify the interfacial properties. However, the model is developed considering only the specific case of a bilinear frictionless bond-slip law. Similarly, the closed-form solution proposed by [39] is based on a bilinear frictionless bond-slip interface law. Although the mathematical background of the two works is similar, the main difference relies on the generalization of the model proposed by [39] to any bond length. Indeed, considering a long bonding length, the model allows a softening-debonding state, whilst for short bonding lengths, the model allows only a softening state before reaching the failure. A further extension of these works was proposed later in [23], with the adoption of a piecewise linear bond-slip interface law comprising a non-zero residual friction. The model was benchmarked against both short and long bonding lengths and adopted for both Near Surface Mounted (NSM) and Externally Bonded (EB) strengthening solutions.

The present work proposes a fully analytical closed-form model in which the interfacial bond-slip relationship is characterized by two branches: (i) a linear elastic phase followed by (ii) an inelastic exponentially decreasing softening behaviour. The advantages with respect to previous closed-form solutions are pivoted to this latter aspect which ensures: (i) a realistic description of the softening branch in a bond-slip law with smoothly decreasing friction as the load increases, (ii) a continuous function representing the softening behaviour during debonding, (iii) few parameters to calibrate the descending branch and finally, (iv) a stable solution even in case of snap backs. Also, the model is intrinsically applicable to any bonding length, allowing the development of three stages: (i) elastic, (ii) mixed elastic/debonding and (iii) debonding.

The present paper is organized as follows: Section 2 discusses the closed-form analytical model here proposed and presents the three possible bonding states: elastic (*Case 1*), mixed elastic-debonding (*Case 2*) and debonding (*Case 3*). Section 3 describes the validation of the analytical model against some experimental studies available in the technical literature and an ongoing collaboration between different Universities. Finally, Section 4 outlines the main conclusions of the present work.

2. The closed-form mathematical model

The mathematical model herein proposed is developed with reference to a FRP strip externally applied on the flat surface of a specimen representing the structural support of the strengthening system (Figure 1). Moreover, since the equations at the basis of the proposed approach are carried out from equilibrium considerations involving an infinitesimal zone of the FRP and specifically considering a debonding mechanism at the reinforcement/support interface without the occurrence of additional phenomena due to damage of the reinforcement nor of the support, the obtained results do not depend on the material composing the support and the input data are related to the reinforcement and the reinforcement/support interface only. Indeed, the following three assumptions were adopted: (i) the strengthening material behaves as elastic during the whole loading process, (ii) all the nonlinearities concentrate at the interface between FRP strip and masonry support (Figure 1-b) and (iii) the FRP-to-support interface is associated only with a Mode II tangential fracture ruled by a $\tau(x) - s(x)$ curve.

Regarding the FRP, the parameters here accounted for are: Young's modulus, E_{FRP}; thickness, t_{FRP}; width, B_{FRP} (see Figure 1-a). On the other hand, regarding the behaviour of the interface, considering the shear stress-slip law showed in Figure 2, the introduced parameters are: bond strength, f_b; slip at the end of the phase 1, s_* and, the rate of fracture energy in the post-peak phase, G_{II}.

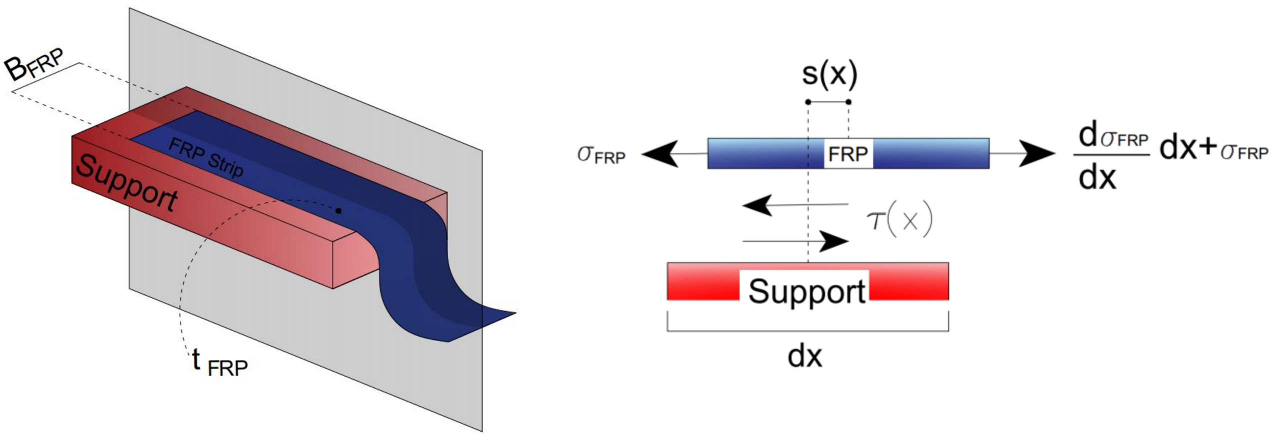

-a -b

Figure 1: Flat FRP strengthening configuration: geometry of the FRP strengthening (-a) and mathematical interface model in case of flat FRP reinforcement (-b).

By imposing the equilibrium along the longitudinal direction on a portion of FRP bonded to the support (Figure 1-b), the following equation is obtained:

$$\frac{d\sigma_{FRP}}{dx} \cdot dx \cdot t_{FRP} \cdot B_{FRP} - \tau(s) \cdot B_{FRP} \cdot dx = 0 \qquad \text{Eq. 1}$$

Considering the assumption (i) related to the constitutive behaviour of the FRP, normal stress of FRP results:

$$\sigma_{FRP} = E_{FRP} \cdot \varepsilon_{FRP}(x) = E_{FRP} \cdot \frac{ds(x)}{dx} \qquad \text{Eq. 2}$$

where: $\varepsilon_{FRP}(x)$ is the axial strain of FRP and $s(x)$ is the relative displacement between the reinforcement and the support, i.e. the slip.

Substituting Eq. 2 into Eq. 1, it results:

$$E_{FRP} \cdot t_{FRP} \cdot \frac{d^2 s(x)}{dx^2} = \tau(s) \qquad \text{Eq. 3}$$

By multiplying both members of Eq. 3 by $\frac{ds(x)}{dx}$, Eq. 4-Eq. 6 are carried out:

$$\frac{1}{2} \cdot \left[2 \cdot \frac{ds(x)}{dx} \cdot \frac{d^2 s(x)}{dx^2} \right] = \frac{\tau(s)}{E_{FRP} \cdot t_{FRP}} \cdot \frac{ds(x)}{dx} \qquad \text{Eq. 4}$$

$$\frac{ds(x)}{dx} = \sqrt{\frac{2}{E_{FRP} \cdot t_{FRP}} \cdot \int \tau(s)\, ds} \qquad \text{Eq. 5}$$

$$\int \frac{ds(x)}{\frac{2}{E_{FRP} \cdot t_{FRP}} \cdot \int \tau(s) ds} = \int dx \qquad \text{Eq. 6}$$

In the present study, the nonlinear piecewise relationship depicted in Figure 2 was selected to describe the behaviour of the specimen at the interface between FRP strengthening and support.

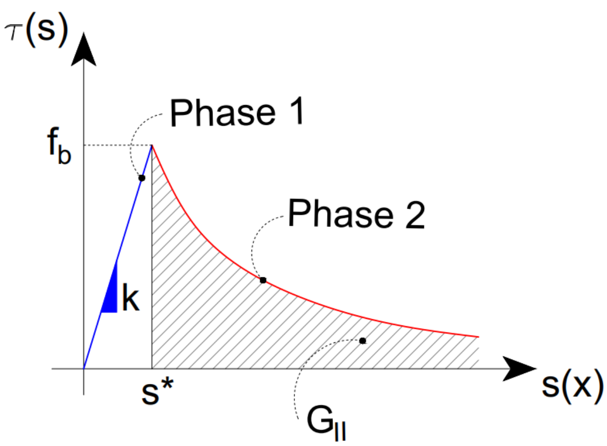

Figure 2: Tangential stress-slip relationship at the interface between FRP strengthening and support.

The relationship $\tau(s) - s(x)$ is composed of two braches identifying two different phases of the behaviour of the interfaces: Phase 1, where a linear phase characterizes the behaviour of the interface until the peak tangential stress f_b is reached (see Eq. 7); Phase 2 where a nonlinear softening branch characterizes the post-peak behaviour of the interface (see Eq. 8):

$$\tau(s) = ks(x) \qquad \text{Eq. 7}$$

$$\tau(s) = f_b \cdot e^{\frac{-(s-s_*)\cdot f_b}{G_{II}}} = \tau_0 \cdot e^{-\frac{s \cdot f_b}{G_{II}}}, \text{ with } \tau_0 = f_b \cdot e^{\frac{s_* f_b}{G_{II}}} \qquad \text{Eq. 8}$$

where: k is the slope of the linear branch; f_b identifies the peak tangential strength at the interface; G_{II} stands for the rate of fracture energy associated with Mode II in the post-peak stage; s_* is the slip value at the end of the phase 1.

The assumptions at the basis of the proposed approach and the type of selected shear stress-slip law for the interface, allow to identify three possible cases for the behaviour of the specimen. Indeed, depending on the value of the displacement imposed at the loaded edge (at this section it corresponds to the slip, here denoted s_0), the three possible cases are: (i) *Case 1*, Eq. 9 holds for the entire bonding length L_L which behaves as elastic; (ii) *Case 2* is characterized by a mixed interface response: only a portion of the bonding length, herein identified as $\tilde{L}$, behaves as elastic, whilst the other one lies in phase 2, Eq. 10; *Case 3*, characterized by L_L (i.e. the entire bonding length) behaving in phase 2 (Eq. 11).

$$0 \leq s_0 < \frac{2s_*}{e^{-\alpha L_L} + e^{\alpha L_L}}$$ *Case 1* Eq. 9

$$\frac{2s_*}{e^{-\alpha L_L} + e^{\alpha L_L}} \leq s_0 \leq s_*$$ *Case 2* Eq. 10

$$s_0 > s_*$$ *Case 3* Eq. 11

Where $\alpha^2 = \frac{k}{E_{FRP} \cdot t_{FRP}}$. In the following the solution of the proposed analytical approach is then provided for the three identified cases.

2.1 Case 1

Since *Case 1* is characterized by a maximum value of slip lower than s_*, the phase I of the law $\tau(s) - s(x)$, i.e. the one described by Eq. 6, distinguished the behaviour of the interface along the whole bond length. Thus, after trivial manipulations, Eq. 12 is obtained. The solution of which is expressed in Eq. 15 provided that α^2 is expressed as Eq. 13 and replaced in Eq. 14.

$$\frac{d^2 s(x)}{dx^2} = \frac{k}{E_{FRP} \cdot t_{FRP}} \cdot s$$ Eq. 12

$$\alpha^2 = \frac{k}{E_{FRP} \cdot t_{FRP}}$$ Eq. 13

$$\frac{d^2 s(x)}{dx^2} - \alpha^2 \cdot s(x) = 0$$ Eq. 14

$$s(x) = A_1 e^{-\alpha x} + A_2 e^{\alpha x}$$ Eq. 15

where A_1 and A_2 are two constants to be determined.

By imposing the conditions at the loaded edge (i.e., $s(0) = s_0$), A_1 is obtained (Eq. 16) as a function on A_2:

$$A_1 = s_0 - A_2 \qquad \text{Eq. 16}$$

$$A_1 = \frac{s_0}{2} = A_2 \qquad \text{Eq. 17}$$

The constants A_1 and A_2 (Eq. 17) are obtained by imposing $\sigma_{FRP} = \frac{ds}{dx} \cdot E_{FRP} = E_{FRP} \cdot \alpha \cdot (A_2 e^{\alpha x} - A_1 e^{-\alpha x}) = 0$ when x=0 and then substituting the relationship between A1 and A2 into Eq. 16.

Finally, the slip $s(x)$ and normal stress in the FRP strengthening σ_{FRP} are obtained (Eq. 18 and Eq. 19 respectively):

$$s(x) = \frac{s_0}{2} \cdot (e^{-\alpha x} + e^{\alpha x}) \qquad \text{Eq. 18}$$

$$\sigma_{FRP} = E_{FRP} \cdot \frac{ds(x)}{dx} = E_{FRP} \cdot \alpha \cdot \frac{s_0}{2} \cdot (e^{\alpha x} - e^{\alpha x}) \qquad \text{Eq. 19}$$

2.2 Case 2

Case 2 is characterized by a behaviour of the interface where both phases 1 and 2 coexist on the bonding length L_L. Therefore Eq. 6 is used providing that the integral of $\tau(s)$ described by Eq. 8 is used, as shown in Eq. 20-Eq. 21:

$$\int \tau(s)\, ds = \int \tau_0 \cdot e^{-\frac{s \cdot f_b}{G_{II}}} ds = -\frac{\tau_0}{f_b} \cdot G_{II} \cdot e^{-\frac{s \cdot f_b}{G_{II}}} + C_1 \qquad \text{Eq. 20}$$

$$\frac{ds}{dx} = \sqrt{\frac{2\tau_0 \cdot G_{II}}{E_{FRP} \cdot t_{FRP} \cdot f_b} \cdot \left(-e^{-\frac{s \cdot f_b}{G_{II}}} + C_1\right)} \qquad \text{Eq. 21}$$

The solution of Eq. 21 is presented in Eq. 22:

$$atanh\left(\sqrt{1 - \frac{e^{-\xi}}{C_1}}\right) = \frac{\sqrt{C_1} \cdot k_1}{2} \cdot x + C_2 \qquad \text{Eq. 22}$$

where: $\xi = \frac{s(x) \cdot f_b}{G_{II}}$, while $k_1 = \sqrt{\frac{2\tau_0 f_b}{E_{FRP} \cdot t_{FRP} \cdot G_{II}}}$.

To find the values of the two constants C_1 and C_2, the following Initial Condition might be applied, which implies that $\frac{ds(x)}{dx} \cdot E_{FRP} = \tilde{\sigma}_{FRP}$ (Eq. 23-Eq. 24):

$$\frac{ds(x)}{dx} \cdot E_{FRP} = \sigma_{FRP}(\tilde{L}) = \frac{s_0}{2} \cdot \alpha \cdot E_{FRP} \cdot \left(e^{\alpha \tilde{L}} - e^{-\alpha \tilde{L}}\right) = \tilde{\sigma}_{FRP} \quad \text{Eq. 23}$$

$$\frac{ds(x)}{dx} \cdot E_{FRP} = \sqrt{\frac{2\tau_0 \cdot E_{FRP} \cdot G_{II}}{t_{FRP} \cdot f_b} \cdot \left(-e^{-\frac{s \cdot f_b}{G_{II}}} + C_1\right)} \quad \text{Eq. 24}$$

Finally, the following value of C_1 (Eq. 25) is obtained:

$$C_1 = e^{\xi_0} + \tilde{\sigma}_{FRP}^2 \cdot \frac{t_{FRP} \cdot f_b}{2E_{FRP} \cdot \tau_0 \cdot G_{II}} \quad \text{Eq. 25}$$

where $\xi_0 = \frac{s_* \cdot f_b}{G_{II}}$. The value of C_2 (Eq. 26) is obtained using Eq. 22 knowing the value of C_1.

$$C_2 = atanh\left(\sqrt{1 - \frac{e^{\xi_0}}{C_1}}\right) \quad \text{Eq. 26}$$

Then, considering the values of the two constants C_1 and C_2, it is possible to derive S_L and σ_{FRP}, which are reported in Eq. 27 and Eq. 28, respectively.

$$S_L = -\frac{G_{II}}{f_b} \cdot ln\left\{C_1\left[1 - tanh^2\left(\frac{\sqrt{C_1} \cdot k_1 \cdot (L - \tilde{L})}{2} + C_2\right)\right]\right\} \quad \text{Eq. 27}$$

$$\sigma_{FRP} = \sqrt{\frac{2\tau_0 \cdot G_{II} \cdot E_{FRP}}{t_{FRP} \cdot f_b} \cdot \left(C_1 - e^{-\frac{s(x) \cdot f_b}{G_{II}}}\right)} \quad \text{Eq. 28}$$

where $\tilde{L}$ is derived in closed form in Eq. 29:

$$\tilde{L} = \frac{1}{\alpha} \cdot ln\left(\frac{s^* + \sqrt{s^{*2} - s_0^2}}{s_0}\right) \quad \text{Eq. 29}$$

Analyzing the solution obtained for *Case 2*, still considering the data of the generic specimen accounted for *Case 1* (see Figure 3 and Figure 4), it is possible to observe a nonlinear trend of the normal stress of FRP vs. slip at the loaded edge curve. This curve is characterized by an ascending segment with a significant slope until the load point B, a subsequent smooth segment which assumes a descending trend next to the load point C (this point corresponds to the end of *Case 2*). Indeed, considering the trend of slip s along the bond length at the load points B and C (and the corresponding curves σ_{FRP}-x and τ-x) it is evident that: (i) at the load point B the zone of specimen next to the unloaded end is characterized by negligible values of slips (and then of τ), i.e. a limited zone of the specimen is significantly involved in the bond process (the so called effective length); (ii) at the load point C the behavior of the specimen shows an opposite situation in terms of shear stresses at the interface: negligible values characterize the status of a significant zone of the interface in close proximity to the loaded end. The latter occurrence is then responsible for the softening behavior.

2.3 Case 3

In *Case 3*, i.e. when the phase 2 characterizes the behaviour of the interface along the whole bond length, Eq. 21 is still valid. In this case, the initial condition to be imposed is reported in Eq. 30, where $\xi_0 = \frac{s_0 \cdot f_b}{G_{II}}$.

$$\sigma_{FRP}(s_0) = \sqrt{\frac{2\tau_0 \cdot G_{II} \cdot E_{FRP}}{t_{FRP} \cdot f_b} \cdot \sqrt{C_1 - e^{\xi_o}}} = 0 \qquad \text{Eq. 30}$$

It is useful to point out that $\sigma_{FRP}(s_0)$ in Eq. 30 represents the normal stress on FRP at the free edge, because in Case 3 phase 2 characterizes the behaviour of the interface along the entire bond length.

By imposing Eq. 30, the value of C_1 is obtained, as indicated in Eq. 31, which in turn is used in Eq. 32 to find C_2.

$$C_1 = e^{-\frac{s_0 \cdot f_b}{G_{II}}} \qquad \text{Eq. 31}$$

$$C_2 = atanh\left(\sqrt{1 - \frac{e^{-\xi_0}}{C_1}}\right) \qquad \text{Eq. 32}$$

Finally, by knowing the values of the two constants C_1 and C_2, S_L and σ_{FRP} might be obtained as reported in Eq. 33 and Eq. 34.

$$S_L = -\frac{G_{II}}{f_b} \cdot ln\left\{C_1\left[1 - tanh^2\left(\frac{\sqrt{C_1} \cdot k_1 \cdot L}{2} + C_2\right)\right]\right\} \qquad \text{Eq. 33}$$

$$\sigma_{FRP}^L = \sqrt{\frac{2\tau_0 \cdot G_{II} \cdot E_{FRP}}{t_{FRP} \cdot f_b} \cdot \left(C_1 - e^{-\frac{S_L \cdot f_b}{G_{II}}}\right)} \qquad \text{Eq. 34}$$

Analyzing the solution of the generic specimen still considered for the previous cases, also for *Case 3*, it emerges a behavior in terms of σ_{FRP}-S highlighted by the snap-back phenomenon, where both normal stress and slip at the loaded edge reduce. Indeed, considering the generic load point C, it is possible to observe a reduction of shear stresses: the maximum value of shear stresses along the bond length is lower than the shear strength f_b. Consequently, this implies an unloading status of the FRP with a corresponding reduction of both normal stresses and strains.

As underlined in next sections, this phenomenon is generally not observed from standard shear-lap tests where it is imposed a displacement at the load edge, progressively increased until the failure.

The obtained solution of the equations at the basis of the proposed approach was implemented in Matlab [40] with the twofold goal of analysing it in terms of bond behaviour of a generic specimen and, subsequently, of assessing its reliability with reference to some experimental cases derived from literature (see next sections). According to the proposed analytical model, the input data here accounted for the generic specimen then concern its geometry (B_{FRP}=100 mm; t_{FRP}=0.165 mm; L_L=287.5 mm), the Young's modulus of reinforcement (E_{FRP}=250000 MPa) and the parameters of the FRP/masonry interface law (f_b=1.65 MPa; s_*=0.05 mm; G_{II}=0.2 N/mm). Introducing these parameters into the proposed analytical model, in particular in Eq. 18 and Eq. 19 referring to the *Case 1*, the results in terms of slip *s* along the bond length at different load steps and in terms of corresponding normal stress of reinforcement σ_{FRP} vs. slip at the loaded edge, are graphically presented in Figure 3. In particular, the point A corresponds to the maximum value of load where the whole interface lies in phase I (i.e. the behavior of the specimen is within *Case 1*). As expected, the maximum value of the slip is attained at the loaded edge where assumes the value s_* corresponding to the end of the phase I. The normal stress of the reinforcement at the loaded edge linearly varies until the point A because of the assumption of a linear constitutive law for this component of the strengthening system and the linear shape of the first branch (phase I) of the shear stress-slip law of the interface.

Figure 5 and Figure 6 depict slip s and shear stress distribution maps along the bond length obtained with the proposed approach considering four time-steps, namely points A, B, C and D. It is worth mentioning that the dimensions of the elements (i.e. support, interface and strengthening materials) were scaled to improve the readability of the graphs. As expected, the debonding front propagates from the loaded end toward the free end (see Figure 6-A, -B and -C). While at the end of the analysis (i.e. point D), a clear snap-back phenomenon is observed, especially in Figure 5-D. A snap-back is also visible in the global curve of Figure 3-b. Generally speaking and according to authors experience, it can be affirmed that such snap-back is visible in the majority of the practical cases at the transition between Case 2 and Case 3. As a matter of fact, in Case 3 the interface between FRP and support is all subjected to softening, whereas in Case 2 part of the interface (near the free edge) is still in the elastic phase. The procedure proposed solves in closed form a Cauchy problem where s_0 (i.e. the interface displacement at the free edge) is imposed. As a consequence, s_L (i.e. the interface displacement at the loaded edge) is found as output result. It may occur, especially for short bond lengths, that the observed s_L decreases in Case 3 when compared to that observed in Case 2, as a consequence of the sudden decrease of the load applied. It is not easy to provide quantitative information on the occurrence of snap-back, because such phenomenon depends on several parameters, such as the interface law adopted (i.e. initial elastic stiffness, tangential strength and fracture energy in mode II) and the geometrical properties of the reinforcement (bond length). The results presented in Figure 4 in terms of normal stress of FRP and shear stress of the interface, both plotted along the bond length, also underline for *Case 1* a behavior of the specimen characterized for both normal stress of FRP and shear stress of interface by the attainment of the peak value at the loaded edge and a progressive reduction along the remain bond length.

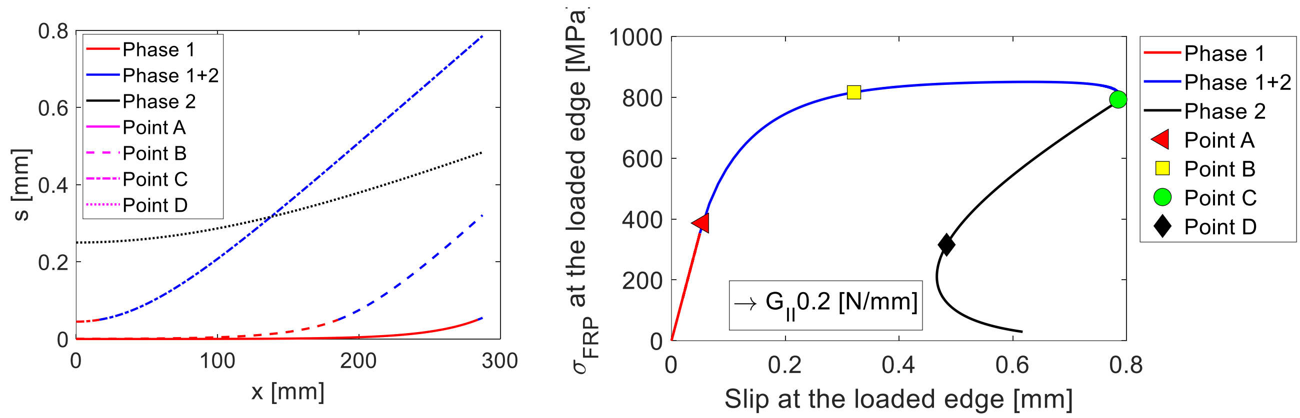

-a -b

Figure 3: Slip *s* distribution along the bond length at different load steps (-a) and normal stress of reinforcement σ_{FRP} vs. slip at the loaded edge (-b) obtained with the proposed approach.

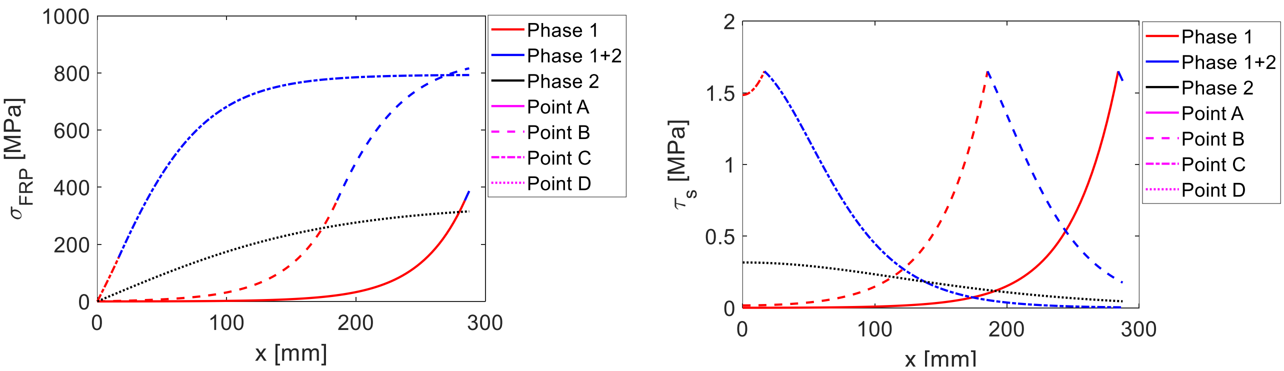

-a -b

Figure 4: Distribution of normal stress of FRP (-a) and shear stress (-b) of the interface along the bond length obtained with the proposed approach.

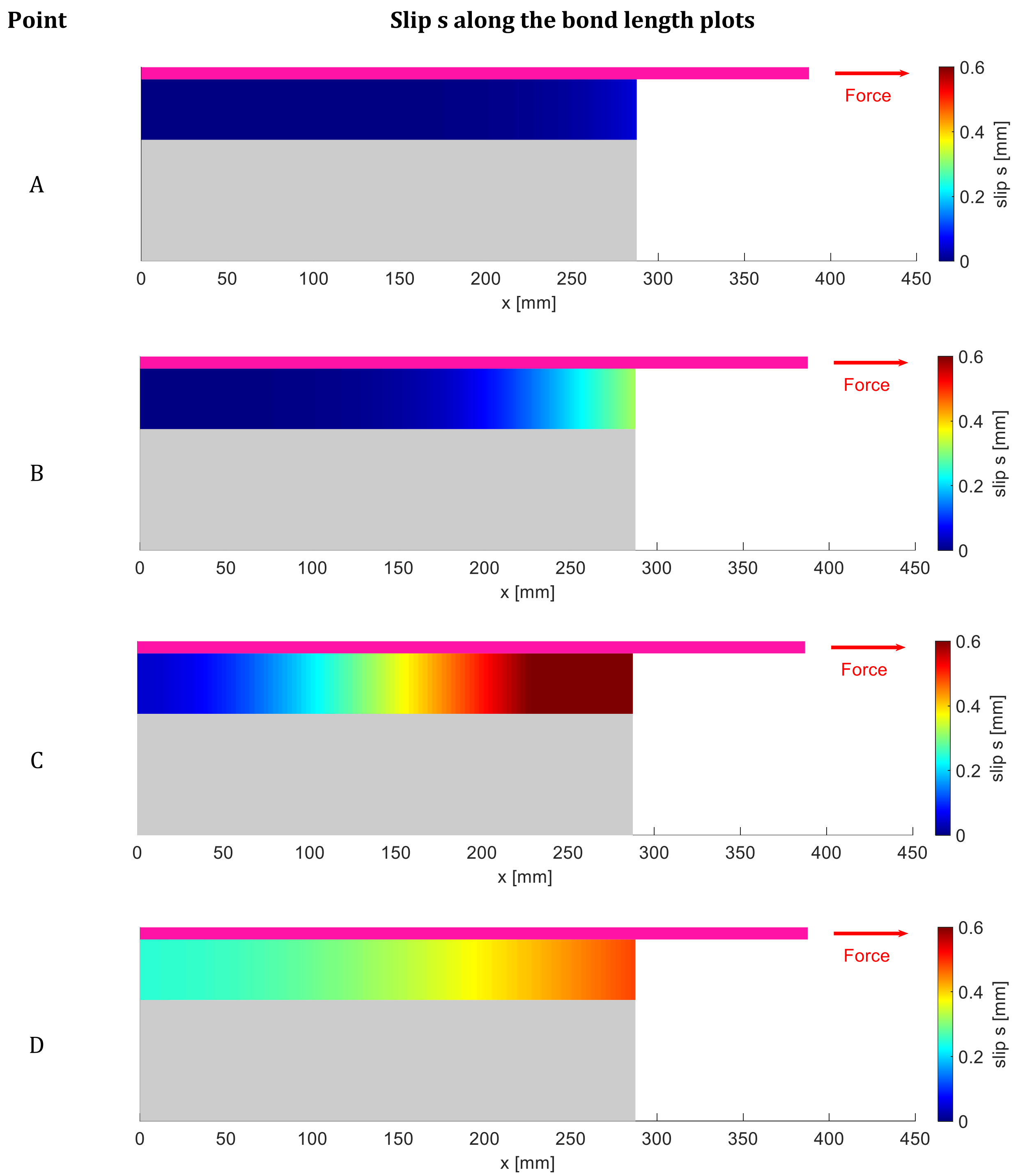

Figure 5: Slip s along the bond length plots considering different load steps.

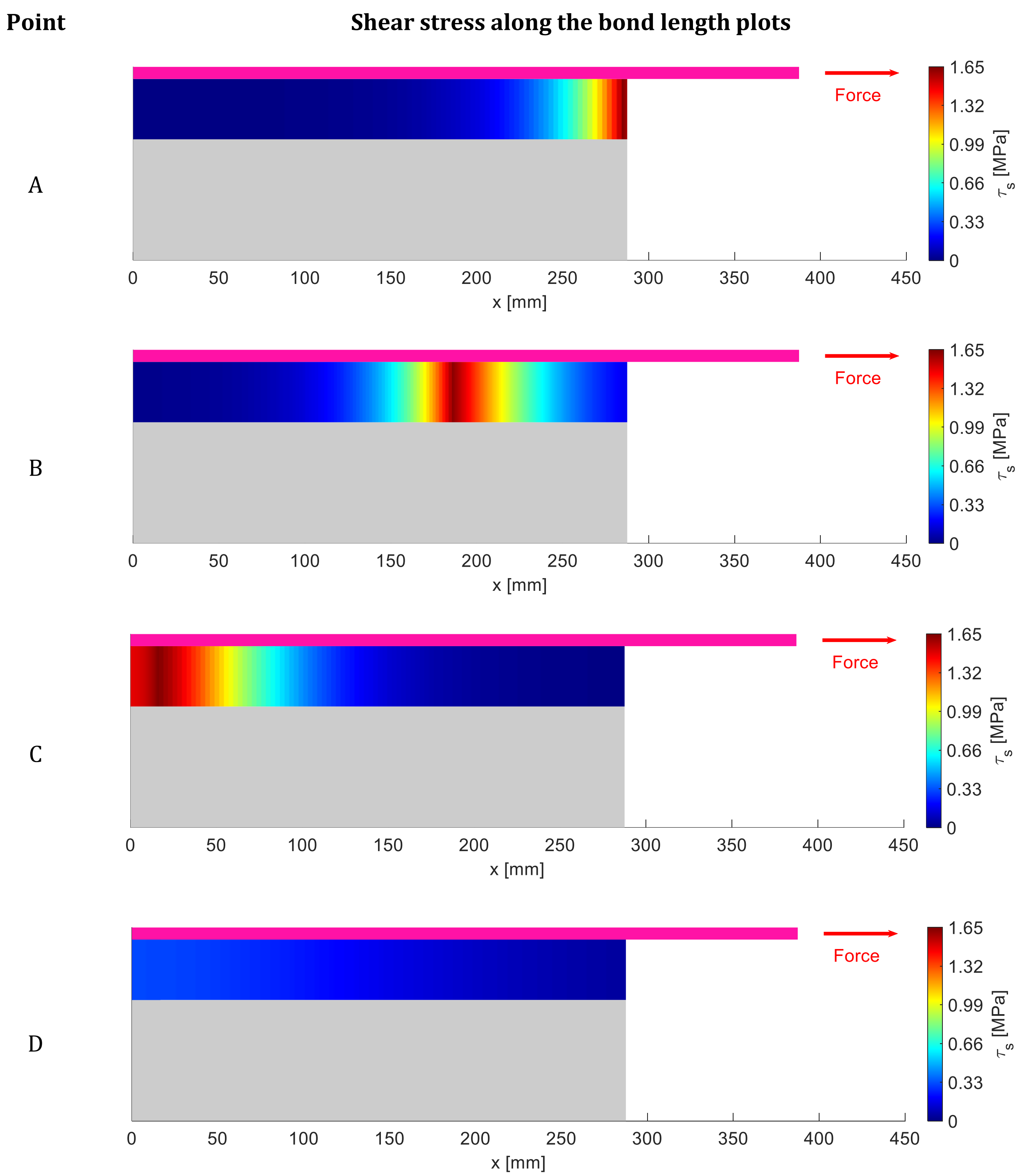

Figure 6: Shear stress maps at the interface along the bond length obtained with the proposed approach.

3. Validation

The proposed approach is here validated by considering shear lap experimental tests of single bricks and brick-mortar assemblages strengthened by FRP derived from studies in the technical literature.

In particular, the first set of specimens refers to the experimental investigation carried out in [13]. They consist of clay bricks strengthened on both sides by a FRP strip bonded to the brick surface for a length *LL* equal to 160mm. Shear lap tests were performed by considering four different types of strengthening materials: carbon (CFRP), glass (GFRP), basalt (BFRP) and steel (SRP). These specimens are labelled in the following as: Valluzzi et al.2012-CFRP (Figure 7); Valluzzi et al.2012-GRFP (Figure 8); Valluzzi et al.2012-BRFP (Figure 9); Valluzzi et al.2012-SRP (Figure 10).

Table 1. Parameters accounted for the validation of the proposed approach.

Label	E_{FRP} [MPa]	t_{FRP} [mm]	B_{FRP} [mm]	f_b [MPa]	s* [mm]	G_{II} [N/mm]	LL [mm]
Valluzzi et al. 2012 – CFRP [13]	233861	0.17	50	2.49	0.016	0.2913	160
Valluzzi et al. 2012 – GFRP [13]	84251	0.12	50	2.49	0.016	0.2789	160
Valluzzi et al. 2012 – BFRP [13]	88397	0.14	50	2.49	0.016	0.2789	160
Valluzzi et al. 2012 – SRP [13]	195054	0.231	50	2.49	0.07	0.2864	160
Rotunno et al. 2018 – CFRP [14]	250000	0.165	100	1.626	0.005	0.2593	330

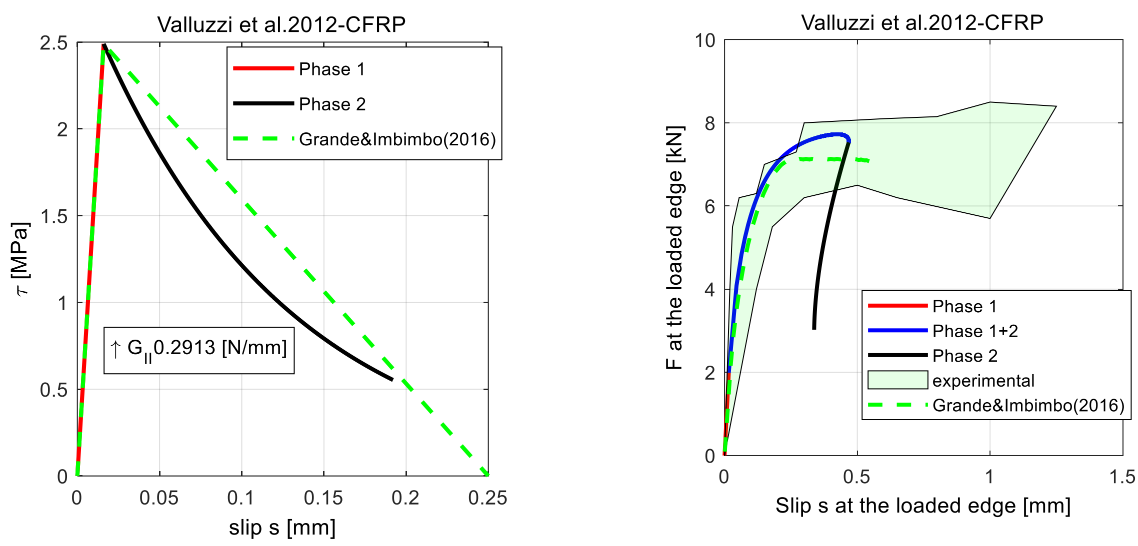

-a -b

Figure 7: Valluzzi et al. 2021-CFRP [13]: Validation of the proposed analytical approach with reference to single brick specimens and different reinforcing materials: reference bi-linear law and obtained equivalent nonlinear law (-a) and experimental, numerical and obtained analytical Force-Slip curves (-b).

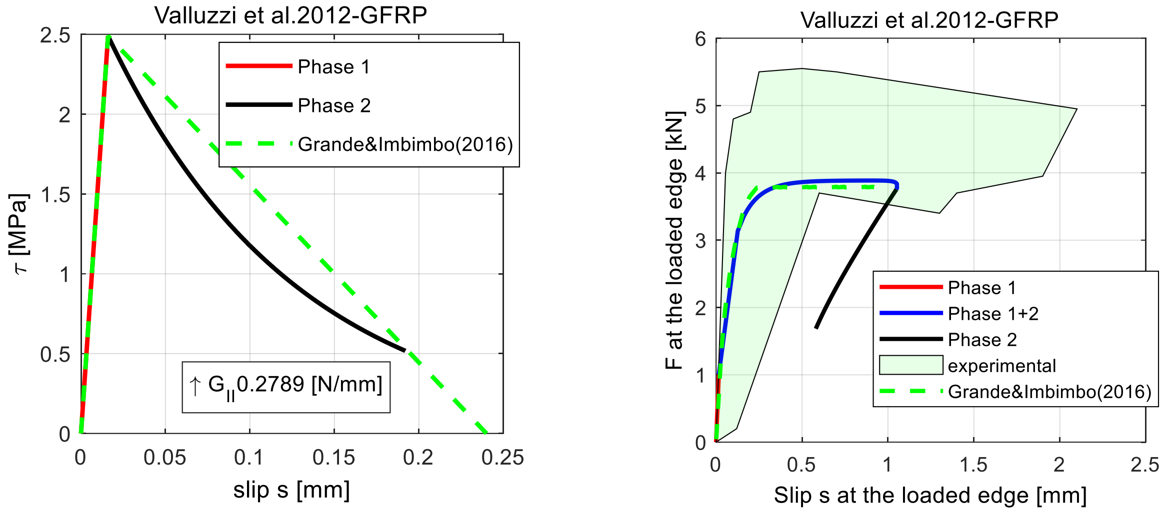

-a -b

Figure 8: Valluzzi et al. 2021-CFRP [13]: Validation of the proposed analytical approach with reference to single brick specimens and different reinforcing materials: reference bi-linear law and obtained equivalent nonlinear law (-a) and experimental, numerical and obtained analytical Force-Slip curves (-b).

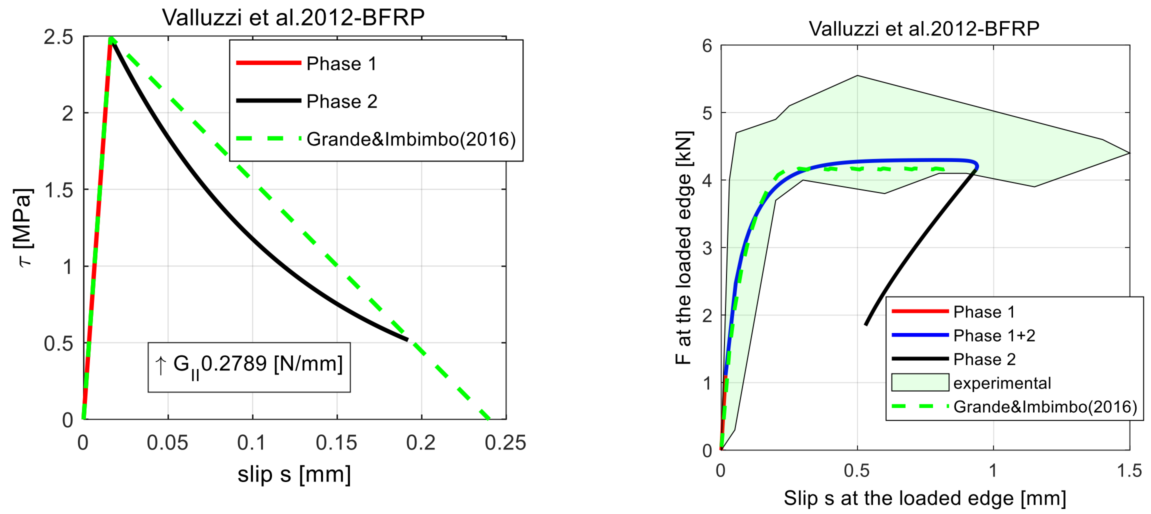

-a -b

Figure 9: Valluzzi et al. 2021-CFRP [13]: Validation of the proposed analytical approach with reference to single brick specimens and different reinforcing materials: reference bi-linear law and obtained equivalent nonlinear law (-a) and experimental, numerical and obtained analytical Force-Slip curves (-b).

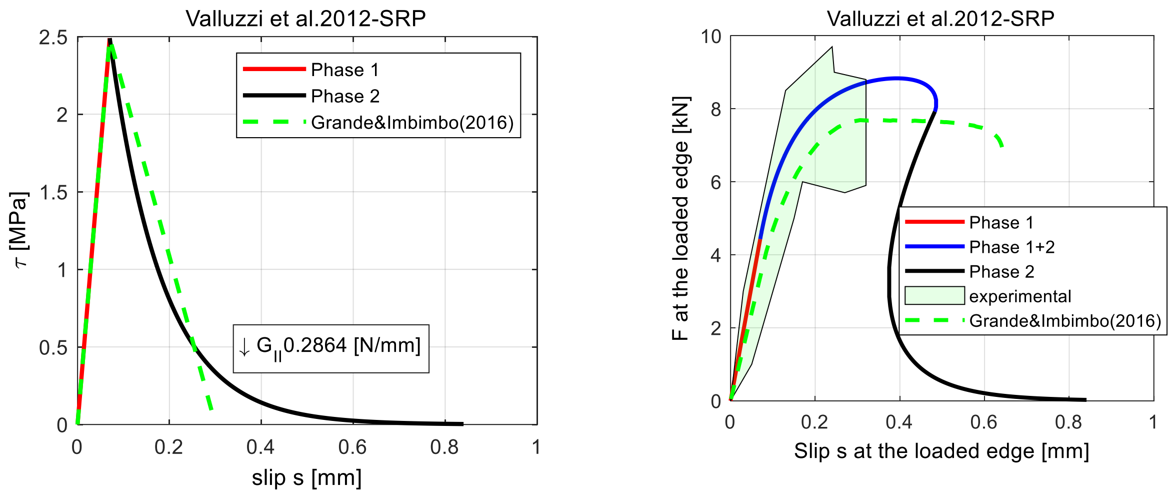

-a -b

Figure 10: Valluzzi et al. 2021-CFRP [13]: Validation of the proposed analytical approach with reference to single brick specimens and different reinforcing materials: reference bi-linear law and obtained equivalent nonlinear law (-a) and experimental, numerical and obtained analytical Force-Slip curves (-b).

Taking into account the simple constitutive shear stress-slip bi-linear law proposed in [17] for characterizing the behaviour of FRP/masonry interface layer, also employed in the numerical study carried out in [16], where the above specimens were specifically accounted for validating a numerical modelling approach denoted *1D spring-model* (see [16] for details), the equivalent shear stress-slip nonlinear law characterizing the analytical approach here proposed has been derived for each specimen (Figure 7-a, Figure 8-a, Figure 9-a and Figure 10-a). Indeed, it has been assumed for the phase 1 the same slope of the ascending branch and the same value of the bond strength of the bi-linear law; for the phase 2 a value of G_{II} equal to the area subtended by the post-peak descending branch of the bi-linear law proposed in [16].

A further case here considered is derived from the experimental study carried out in [14] and also introduced in [41] for developing numerical analyses throughout an interface numerical model valid also in case of curved substrates (see for [41] details). In this case, while the reinforcement is still a carbon fiber strip, the substrate is a masonry pillar composed of five clay bricks with interposed mortar joints made of lime and cement as binder. The reinforcement is applied on one side only of the pillar for a bond length *LL* equal to 330 mm. Also, in this case, the constitutive law of the reinforcement/masonry interface (see Figure 11) has been derived according to the procedure accounted for the previous specimens, by considering the bi-linear law proposed in [18].

The results obtained from the analytical model here proposed are compared with the experimental Force-Slip curves (or envelope areas of experimental curves) and presented in Figure 7-b, Figure 8-b,

Figure 9-b and Figure 10-b for the first set of specimens and in Figure 11 for the masonry pillar specimen.

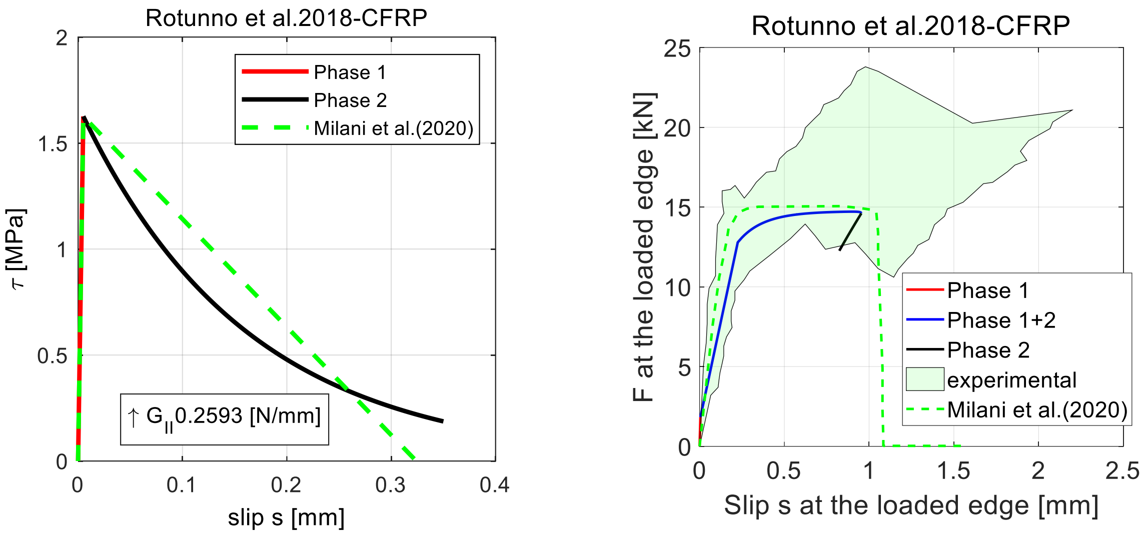

-a -b

Figure 11: Validation of the proposed analytical approach with reference to pillar masonry specimens: reference bi-linear law and obtained equivalent nonlinear law (-a) and experimental, numerical, and obtained analytical Force-Slip curves (-b).

From the plots clearly emerges the efficacy of the proposed analytical approach in predicting the pre-peak phase and the peak load. A good agreement is also observed with respect to the numerical solutions. Nevertheless, while the numerical solutions halt when the equilibrium is no longer satisfied, the analytical solution proceeds by underlying the snap-back phenomenon.

Although in the majority of analysed cases the ultimate experimental displacement results greater than both numerical and analytical ones, as underlined in [16], the post-peak behaviour is generally influenced by phenomena, such as the degradation of the detached zone of the reinforcement, which lead to a greater deformability of the system.

4. Conclusions

This research proposes a fully analytical approach aimed at studying the FRP debonding process from flat brittle surfaces (i.e. masonry prisms). The analytical approach derives from imposing equilibrium considerations involving an infinitesimal zone of the FRP. The approach assumes that all the nonlinearities are concentrated at the interface between FRP, strip and masonry support with FRP-to-support interfaces associated with a Mode II tangential fracture behaviour only.

Based on the results of the present work, the following conclusions can be drawn:

- The proposed closed-form model considers a debonding mechanism at the reinforcement/support interface only.
- The obtained results are decoupled from the material composing the support and the input data are related to the reinforcement/support interface only.
- A closed form solution, characterized by few parameters governing the mathematical problem (interfacial stress-slip law characterized by an initial linear elastic phase followed by an inelastic exponentially decreasing softening behaviour) and a limited computational effort, is provided.
- The approach is benchmarked with two sets of experimental investigations: (i) a laboratory campaign using different reinforcing materials and (ii) an ongoing experimental and numerical research collaboration carried out by the authors.
- The comparisons in terms of force-slip curves clearly highlight the efficacy of the proposed analytical approach in predicting the pre-peak phase and the peak load.
- Compared to other numerical approaches, the analytical solution resulted more stable and able to capture possible snap-back phenomena.

5. References

[1] J. Vaculik, P. Visintin, N.G. Burton, M.C. Griffith, R. Seracino, State-of-the-art review and future research directions for FRP-to-masonry bond research: Test methods and techniques for extraction of bond-slip behaviour, Constr. Build. Mater., v. 183, 2018, pp. 325-345.

[2] N.G. Shrive, The use of fibre reinforced polymers to improve seismic resistance of masonry, Constr. Build. Mater., 20 (4), 2006, pp. 269-277.

[3] M. Corradi, A. Borri, A. Vignoli, Strengthening techniques tested on masonry structures struck by the Umbria–Marche earthquake of 1997–1998, Constr. Build. Mater., 16 (4), 2002, pp. 229-239.

[4] D. Li, J. Zhou, J. Ou, Damage, nondestructive evaluation and rehabilitation of FRP composite-RC structure: A review, Construction and Building Materials, v. 271, 2021.

[5] Y. J. Kim, State of the practice of FRP composites in highway bridges, Engineering Structures, v. 179, 2019, pp. 1-8.

[6] C.E. Bakis, L.C. Bank, V.L. Brown, E. Cosenza, J.F. Davalos, J.J. Lesko, et al., Fiber-reinforced polymer composites for construction—state-of-the-art review, J Compos Constr, 6 (2), 2002, pp. 73-87.

[7] L.C. Hollaway, J.G. Teng, Strengthening and rehabilitation of civil infrastructures using fiber-reinforced polymer (FRP) composites, Woodhead Publishing Limited, Cambridge (England) (2008).

[8] A. M. D'Altri, S. de Miranda, Environmentally-induced loss of performance in FRP strengthening systems bonded to full-scale masonry structures, Construction and Building Materials, v. 249.

[9] P. Zhang, D. Lei, Q. Ren, J. He, H. Shen, Z. Yanga, Experimental and numerical investigation of debonding process of the FRP plate-concrete interface, Constr. Build. Mater., v. 235, 2020.

[10] C. Mazzotti, M. Savoia, B. Ferracuti, An experimental study on delamination of FRP plates bonded to concrete, Constr. Build. Mater., v. 22 (7), 2008, pp. 1409-1421

[11] H.C. Biscaia, C. Chastre, I.S. Borba, et al., Experimental evaluation of bonding between CFRP laminates and different structural materials, J. Compos. Constr., v. 20 (3), 2015.

[12] M.A. Aiello, S.M. Sciolti, Bond analysis of masonry structures strengthened with CFRP sheets, Constr. Build. Mater., v. 20 (1–2), 2006, pp. 90-100.

[13] M.R. Valluzzi, D.V. Oliveira, A. Caratelli, G. Castori, M. Corradi, G. De Felice, et al. Round Robin Test for composite-to-brick shear bond characterization. Mater. Struct. Constr., v. 45, 2012, pp. 1761–1791.

[14] T. Rotunno, M. Fagone, E. Bertolesi, E. Grande, G. Milani, Single lap shear tests of masonry curved pillars externally strengthened by CFRP strips. Compos Struct, v. 200, 2018, pp. 434–448.

[15] T. Rotunno, M. Fagone, E. Bertolesi, E. Grande, G. Milani, Curved masonry pillars reinforced with anchored CFRP sheets: An experimental analysis, Composites Part B: Engineering, v. 174, 2019.

[16] E. Grande, M. Imbimbo, Simple 1D-Finite Element approach for the study of the bond behavior of masonry elements strengthened by FRP. Compos. Part B Eng., v.91, 2016 pp. 548–558.

[17] E. Grande, M. Imbimbo, E. Sacco, Simple Model for Bond Behavior of Masonry Elements Strengthened with FRP, J. Compos. Constr., v. 15, 2011, pp. :354–363.

[18] E. Grande, M. Fagone, T. Rotunno, E. Bertolesi, G. Milani, Coupled interface-based modelling approach for the numerical analysis of curved masonry specimens strengthened by CFRP, Compos. Struct., v.200, 2018, pp. 498–506.

[19] C. Carloni, F. Focacci, FRP-masonry interfacial debonding: an energy balance approach to determine the influence of the mortar joints, Eur. J. Mech. A/Solid., v. 55, 2016, pp. 122-133.

[20] T. Rotunno, L. Rovero, U. Tonietti, S. Briccoli Bati, Experimental study of bond behavior of CFRP-to-brick joints, J. Compos. Constr., v. 19, 2015.

[21] R. Fedele, G. Milani, Assessment of bonding stresses between FRP sheets and masonry pillars during delamination tests, Compos. Part B Eng., v. 43, 2012, pp. 1999-2011.

[22] G. Mazzucco, V.A. Salomoni, C. Pellegrino, C.E. Majorana, Three-dimensional modelling of bond behaviour between concrete and FRP reinforcement, Eng. Comput., v. 28 (1), 2011, pp. 5-29.

[23] J. Vaculik, A.B. Sturm, P. Visintin, M.C. Griffith, Modelling FRP-to-substrate joints using the bilinear bond-slip rule with allowance for friction—full-range analytical solutions for long and short bonded lengths, Int. J. Solid Struct., v. 135, 2018, pp. 245-260.

[24] F. Focacci, C. Carloni, Periodic variation of the transferable load at the FRP-masonry interface, Compos. Struct., v. 129, 2015, pp. 90-100.

[25] M. Malena, F. Focacci, C. Carloni, G. de Felice, The effect of the shape of the cohesive material law on the stress transfer at the FRP-masonry interface, Compos. B Eng., v. 110, 2017, pp. 368-380.

[26] C. Faella, G. Camorani, E. Martinelli, S.O. Paciello, F. Perri, Bond behaviour of FRP strips glued on masonry: Experimental investigation and empirical formulation, Constr. Build. Mater., v. 31, 2012, pp. 353-363.

[27] CNR-DT 200 R1-2013, Guide for the Design and Construction of Externally Bonded FRP Systems for Strengthening Existing Structures, National Research Council, Italy 2013.

[28] ACI 440.7R-10, Guide for the Design and Construction of Externally Bonded fibre-Reinforced Polymer Systems for Strengthening Unreinforced Masonry Structures, American Concrete Institute, Farmington Hills, MI, US 2010.

[29] TR 55 Design guidance for strengthening concrete structures using fibre composite materials. 3rd edition (includes Amendment No. 1 dated October 2013), The Concrete Society (UK) 2000.

[30] Fib Bulletin 14: Externally Bonded FRP Reinforcement for RC Structures, fédération internationale du béton, Lausanne, Switzerland, 2001.
[31] ISIS Design Manual No. 4, Strengthening Reinforced Concrete Structures with Externally-Bonded Fibre Reinforced Polymers (FRPs). ISIS Canada.
[32] JSCE, 2001, Recommendation for Upgrading of Concrete Structures with use of Continuous Fiber Sheets, Concrete Engineering Series 41, Japan Society of Civil Engineers, Tokyo, Japan.
[33] R. Fedele, G. Milani, Three-dimensional effects induced by FRP-from-masonry delamination, Composite Structures, v. 93 (7), 2011, pp. 1819-1831.
[34] R. Fedele, G. Milani, A numerical insight into the response of masonry reinforced by FRP strips: the case of perfect adhesion, Compos Struct, 92, 2010, pp. 2345-2357.
[35] E. Bertolesi, G. Milani, M. Fagone, T. Rotunno, E. Grande, Heterogeneous FE model for single lap shear tests on FRP reinforced masonry curved pillars with spike anchors, Constr. and Build. Mat., v. 258, 2020.
[36] E. Bertolesi, G. Milani, M. Fagone, T. Rotunno, E. Grande, Micro-mechanical FE numerical model for masonry curved pillars reinforced with FRP strips subjected to single lap shear tests, Composite Structures, v. 201, 2018, pp. 916-931.
[37] B. Ghiassi, D.V. Oliveira, P.B. Lourenço, G. Marcari, Numerical study of the role of mortar joints in the bond behavior of FRP-strengthened masonry, Composites: Part B., 46, 2013, pp. 21-30.
[38] H. Yuana, J.G. Teng, R. Seracino, Z.S. Wu, J. Yao, Full-range behavior of FRP-to-concrete bonded joints, Engineering Structures, v. 26 (5), 2004, pp. 553-565.
[39] A. Caggiano, E. Martinelli, C. Faella, A fully-analytical approach for modelling the response of FRP plates bonded to a brittle substrate, International Journal of Solids and Structures, v. 49 (17), 2012, pp. 2291-2300.
[40] MATLAB version 7.10.0. Natick, Massachusetts: The MathWorks Inc.; 2010.
[41] G. Milani, M. Fagone, T. Rotunno, E. Grande, E. Bertolesi, Development of an interface numerical model for C-FRPs applied on flat and curved masonry pillars, Compos. Struct., v. 241, 2020.